Search for $B_s^0 - \overline{B}_s^0$ oscillations

DELPHI Collaboration

W. Adam [aw], T. Adye [aj], I. Ajinenko [ao], G.D. Alekseev [p], R. Alemany [av],
P.P. Allport [v], S. Almehed [x], U. Amaldi [i], S. Amato [at], P. Andersson [aq],
A. Andreazza [i], P. Antilogus [i], W-D. Apel [q], Y. Arnoud [n], B. Åsman [aq],
J-E. Augustin [y], A. Augustinus [ad], P. Baillon [i], P. Bambade [s], F. Barao [u],
M. Barbi [at], D.Y. Bardin [p], G. Barker [i], A. Baroncelli [am], O. Barring [x], M.J. Bates [aj],
M. Battaglia [o], M. Baubillier [w], J. Baudot [al], K-H. Becks [ay], M. Begalli [f],
P. Beilliere [h], Yu. Belokopytov [i,l], K. Belous [ao], A.C. Benvenuti [e], C. Berat [n],
M. Berggren [at], D. Bertini [y], D. Bertrand [b], M. Besancon [al], F. Bianchi [ar], M. Bigi [ar],
M.S. Bilenky [p], P. Billoir [w], M-A. Bizouard [s], D. Bloch [j], M. Blume [ay],
M. Bonesini [aa], W. Bonivento [aa], M. Boonekamp [al], P.S.L. Booth [v], A.W. Borgland [d],
G. Borisov [al,ao], C. Bosio [am], O. Botner [au], E. Boudinov [ad], B. Bouquet [s],
C. Bourdarios [s], T.J.V. Bowcock [v], I. Bozovic [k], M. Bozzo [m], P. Branchini [am],
K.D. Brand [ai], T. Brenke [ay], R.A. Brenner [au], R.C.A. Brown [i], P. Bruckman [r],
J-M. Brunet [h], L. Bugge [af], T. Buran [af], T. Burgsmueller [ay], P. Buschmann [ay],
S. Cabrera [av], M. Caccia [aa], M. Calvi [aa], A.J. Camacho Rozas [an], T. Camporesi [i],
V. Canale [ak], M. Canepa [m], F. Carena [i], L. Carroll [v], C. Caso [m],
M.V. Castillo Gimenez [av], A. Cattai [i], F.R. Cavallo [e], V. Chabaud [i], M. Chapkin [ao],
Ph. Charpentier [i], L. Chaussard [y], P. Checchia [ai], G.A. Chelkov [p], M. Chen [b],
R. Chierici [ar], P. Chliapnikov [ao], P. Chochula [g], V. Chorowicz [y], J. Chudoba [ac],
V. Cindro [ap], P. Collins [i], M. Colomer [av], R. Contri [m], E. Cortina [av], G. Cosme [s],
F. Cossutti [as], J-H. Cowell [v], H.B. Crawley [a], D. Crennell [aj], G. Crosetti [m],
J. Cuevas Maestro [ag], S. Czellar [o], J. Dahm [ay], B. Dalmagne [s], G. Damgaard [ab],
P.D. Dauncey [aj], M. Davenport [i], W. Da Silva [w], A. Deghorain [b], G. Della Ricca [as],
P. Delpierre [z], N. Demaria [ah], A. De Angelis [i], W. De Boer [q], S. De Brabandere [b],
C. De Clercq [b], C. De La Vaissiere [w], B. De Lotto [as], A. De Min [ai], L. De Paula [at],
H. Dijkstra [i], L. Di Ciaccio [ak], A. Di Diodato [ak], A. Djannati [h], J. Dolbeau [h],
K. Doroba [ax], M. Dracos [j], J. Drees [ay], K.-A. Drees [ay], M. Dris [ae], J-D. Durand [y,i],

D. Edsall [a], R. Ehret [q], G. Eigen [d], T. Ekelof [au], G. Ekspong [aq], M. Elsing [i],
J-P. Engel [j], B. Erzen [ap], M. Espirito Santo [u], E. Falk [x], G. Fanourakis [k],
D. Fassouliotis [as], M. Feindt [i], P. Ferrari [aa], A. Ferrer [av], S. Fichet [w], T.A. Filippas [ae],
A. Firestone [a], P.-A. Fischer [j], H. Foeth [i], E. Fokitis [ae], F. Fontanelli [m],
F. Formenti [i], B. Franek [aj], A.G. Frodesen [d], R. Fruhwirth [aw], F. Fulda-Quenzer [s],
J. Fuster [av], A. Galloni [v], D. Gamba [ar], M. Gandelman [at], C. Garcia [av], J. Garcia [an],
C. Gaspar [i], U. Gasparini [ai], Ph. Gavillet [i], E.N. Gazis [ae], D. Gele [j], J-P. Gerber [j],
L. Gerdyukov [ao], R. Gokieli [ax], B. Golob [ap], P. Goncalves [u], G. Gopal [aj], L. Gorn [a],
M. Gorski [ax], Yu. Gouz [ar,1], V. Gracco [m], E. Graziani [am], C. Green [v], A. Grefrath [ay],
P. Gris [al], G. Grosdidier [s], K. Grzelak [ax], M. Gunther [au], J. Guy [aj], F. Hahn [i],
S. Hahn [ay], Z. Hajduk [r], A. Hallgren [au], K. Hamacher [ay], F.J. Harris [ah], V. Hedberg [x],
R. Henriques [u], J.J. Hernandez [av], P. Herquet [b], H. Herr [i], T.L. Hessing [ah],
J.-M. Heuser [ay], E. Higon [av], S-O. Holmgren [aq], P.J. Holt [ah], D. Holthuizen [ad],
S. Hoorelbeke [b], M. Houlden [v], J. Hrubec [aw], K. Huet [b], K. Hultqvist [aq],
J.N. Jackson [v], R. Jacobsson [aq], P. Jalocha [i], R. Janik [g], Ch. Jarlskog [x],
G. Jarlskog [x], P. Jarry [al], B. Jean-Marie [s], E.K. Johansson [aq], L. Jonsson [x],
P. Jonsson [x], C. Joram [i], P. Juillot [j], M. Kaiser [q], F. Kapusta [w], K. Karafasoulis [k],
E. Karvelas [k], S. Katsanevas [y], E.C. Katsoufis [ae], R. Keranen [d], Yu. Khokhlov [ao],
B.A. Khomenko [p], N.N. Khovanski [p], B. King [v], N.J. Kjaer [ad], O. Klapp [ay],
H. Klein [i], P. Kluit [ad], D. Knoblauch [q], B. Koene [ad], P. Kokkinias [k], M. Koratzinos [i],
K. Korcyl [r], V. Kostioukhine [ao], C. Kourkoumelis [c], O. Kouznetsov [p],
M. Krammer [aw], C. Kreuter [i], I. Kronkvist [x], Z. Krumstein [p], W. Krupinski [r],
P. Kubinec [g], W. Kucewicz [r], K. Kurvinen [o], C. Lacasta [i], I. Laktineh [y],
J.W. Lamsa [a], L. Lanceri [as], D.W. Lane [a], P. Langefeld [ay], J-P. Laugier [al],
R. Lauhakangas [o], G. Leder [aw], F. Ledroit [n], V. Lefebure [b], C.K. Legan [a],
A. Leisos [k], R. Leitner [ac], J. Lemonne [b], G. Lenzen [ay], V. Lepeltier [s], T. Lesiak [r],
M. Lethuillier [al], J. Libby [ah], D. Liko [i], A. Lipniacka [aq], I. Lippi [ai], B. Loerstad [x],
J.G. Loken [ah], J.M. Lopez [an], D. Loukas [k], P. Lutz [al], L. Lyons [ah],
J. MacNaughton [aw], G. Maehlum [q], J.R. Mahon [f], A. Maio [u], T.G.M. Malmgren [aq],
V. Malychev [p], F. Mandl [aw], J. Marco [an], R. Marco [an], B. Marechal [at], M. Margoni [ai],
J-C. Marin [i], C. Mariotti [i], A. Markou [k], C. Martinez-Rivero [ag], F. Martinez-Vidal [av],
S. Marti i Garcia [v], J. Masik [ac], F. Matorras [an], C. Matteuzzi [aa], G. Matthiae [ak],
M. Mazzucato [ai], M. Mc Cubbin [v], R. Mc Kay [a], R. Mc Nulty [i], G. Mc Pherson [v],
J. Medbo [au], M. Merk [ad], C. Meroni [aa], S. Meyer [q], W.T. Meyer [a], M. Michelotto [ai],
E. Migliore [ar], L. Mirabito [y], W.A. Mitaroff [aw], U. Mjoernmark [x], T. Moa [aq],
R. Moeller [ab], K. Moenig [i], M.R. Monge [m], P. Morettini [m], H. Mueller [q],
K. Muenich [ay], M. Mulders [ad], L.M. Mundim [f], W.J. Murray [aj], B. Muryn [n,r],
G. Myatt [ah], T. Myklebust [af], F. Naraghi [n], F.L. Navarria [e], S. Navas [av],

K. Nawrocki [ax], P. Negri [aa], S. Nemecek [l], W. Neumann [ay], N. Neumeister [aw],
R. Nicolaidou [c], B.S. Nielsen [ab], M. Nieuwenhuizen [ad], V. Nikolaenko [j],
M. Nikolenko [j,p], P. Niss [aq], A. Nomerotski [ai], A. Normand [v], A. Nygren [x],
W. Oberschulte-Beckmann [q], V. Obraztsov [ao], A.G. Olshevski [p], A. Onofre [u],
R. Orava [o], G. Orazi [j], S. Ortuno [av], K. Osterberg [o], A. Ouraou [al], P. Paganini [s],
M. Paganoni [i,aa], S. Paiano [e], R. Pain [w], H. Palka [r], Th.D. Papadopoulou [ae],
K. Papageorgiou [k], L. Pape [i], C. Parkes [ah], F. Parodi [m], U. Parzefall [v], A. Passeri [am],
M. Pegoraro [ai], L. Peralta [u], H. Pernegger [aw], M. Pernicka [aw], A. Perrotta [e],
C. Petridou [as], A. Petrolini [m], H.T. Phillips [aj], G. Piana [m], F. Pierre [al], M. Pimenta [u],
E. Piotto [ai], T. Podobnik [ah], O. Podobrin [i], M.E. Pol [f], G. Polok [r], P. Poropat [as],
V. Pozdniakov [p], P. Privitera [ak], N. Pukhaeva [p], A. Pullia [aa], D. Radojicic [ah],
S. Ragazzi [aa], H. Rahmani [ae], P.N. Ratoff [t], A.L. Read [af], M. Reale [ay], P. Rebecchi [i],
N.G. Redaelli [aa], M. Regler [aw], D. Reid [i], R. Reinhardt [ay], P.B. Renton [ah],
L.K. Resvanis [c], F. Richard [s], J. Ridky [l], G. Rinaudo [ar], O. Rohne [af], A. Romero [ar],
P. Ronchese [ai], L. Roos [w], E.I. Rosenberg [a], P. Rosinsky [g], P. Roudeau [s],
T. Rovelli [e], W. Ruckstuhl [ad], V. Ruhlmann-Kleider [al], A. Ruiz [an], K. Rybicki [r],
H. Saarikko [o], Y. Sacquin [al], A. Sadovsky [p], G. Sajot [n], J. Salt [av], M. Sannino [m],
H. Schneider [q], U. Schwickerath [q], M.A.E. Schyns [ay], G. Sciolla [ar], F. Scuri [as],
P. Seager [t], Y. Sedykh [p], A.M. Segar [ah], A. Seitz [q], R. Sekulin [aj], L. Serbelloni [ak],
R.C. Shellard [f], A. Sheridan [v], I. Siccama [ad], P. Siegrist [i,al], R. Silvestre [al],
F. Simonetto [ai], A.N. Sisakian [p], T.B. Skaali [af], G. Smadja [y], N. Smirnov [ao],
O. Smirnova [x], G.R. Smith [aj], O. Solovianov [ao], R. Sosnowski [ax], D. Souza-Santos [f],
T. Spassov [u], E. Spiriti [am], P. Sponholz [ay], S. Squarcia [m], D. Stampfer [i],
C. Stanescu [am], S. Stanic [ap], S. Stapnes [af], I. Stavitski [ai], K. Stevenson [ah],
A. Stocchi [s], J. Strauss [aw], R. Strub [j], B. Stugu [d], M. Szczekowski [ax],
M. Szeptycka [ax], T. Tabarelli [aa], J.P. Tavernet [w], O. Tchikilev [ao], F. Tegenfeldt [au],
F. Terranova [aa], J. Thomas [ah], A. Tilquin [z], J. Timmermans [ad], L.G. Tkatchev [p],
T. Todorov [j], S. Todorova [j], D.Z. Toet [ad], A. Tomaradze [b], B. Tome [u],
A. Tonazzo [aa], L. Tortora [am], G. Transtromer [x], D. Treille [i], G. Tristram [h],
A. Trombini [s], C. Troncon [aa], A. Tsirou [i], M-L. Turluer [al], I.A. Tyapkin [p],
M. Tyndel [aj], S. Tzamarias [k], B. Ueberschaer [ay], O. Ullaland [i], V. Uvarov [ao],
G. Valenti [e], E. Vallazza [as], G.W. Van Apeldoorn [ad], P. Van Dam [ad], J. Van Eldik [ad],
A. Van Lysebetten [b], N. Vassilopoulos [ah], G. Vegni [aa], L. Ventura [ai], W. Venus [aj],
F. Verbeure [b], M. Verlato [ai], L.S. Vertogradov [p], D. Vilanova [al], P. Vincent [y],
L. Vitale [as], E. Vlasov [ao], A.S. Vodopyanov [p], V. Vrba [l], H. Wahlen [ay], C. Walck [aq],

---

F. Waldner [as], C. Weiser [q], A.M. Wetherell [i], D. Wicke [ay], J.H. Wickens [b],
M. Wielers [q], G.R. Wilkinson [i], W.S.C. Williams [ah], M. Winter [j], M. Witek [r],
T. Wlodek [s], J. Yi [a], K. Yip [ah], O. Yushchenko [ao], F. Zach [y], A. Zaitsev [ao],
A. Zalewska [i], P. Zalewski [ax], D. Zavrtanik [ap], E. Zevgolatakos [k], N.I. Zimin [p],
G.C. Zucchelli [aq], G. Zumerle [ai]

[a] Department of Physics and Astronomy, Iowa State University, Ames IA 50011-3160, USA
[b] Physics Department, Univ. Instelling Antwerpen, Universiteitsplein 1, B-2610 Wilrijk, Belgium
and IIHE, ULB-VUB, Pleinlaan 2, B-1050 Brussels, Belgium
and Faculté des Sciences, Univ. de l'Etat Mons, Av. Maistriau 19, B-7000 Mons, Belgium
[c] Physics Laboratory, University of Athens, Solonos Str. 104, GR-10680 Athens, Greece
[d] Department of Physics, University of Bergen, Allégaten 55, N-5007 Bergen, Norway
[e] Dipartimento di Fisica, Università di Bologna and INFN, Via Irnerio 46, I-40126 Bologna, Italy
[f] Centro Brasileiro de Pesquisas Físicas, rua Xavier Sigaud 150, RJ-22290 Rio de Janeiro, Brazil
and Depto. de Física, Pont. Univ. Católica, C.P. 38071 RJ-22453 Rio de Janeiro, Brazil
and Inst. de Física, Univ. Estadual do Rio de Janeiro, rua São Francisco Xavier 524, Rio de Janeiro, Brazil
[g] Comenius University, Faculty of Mathematics and Physics, Mlynska Dolina, SK-84215 Bratislava, Slovakia
[h] Collège de France, Lab. de Physique Corpusculaire, IN2P3-CNRS, F-75231 Paris Cedex 05, France
[i] CERN, CH-1211 Geneva 23, Switzerland
[j] Institut de Recherches Subatomiques, IN2P3 - CNRS / ULP - BP20, F-67037 Strasbourg Cedex, France
[k] Institute of Nuclear Physics, N.C.S.R. Demokritos, P.O. Box 60228, GR-15310 Athens, Greece
[l] FZU, Inst. of Physics of the C.A.S. High Energy Physics Division, Na Slovance 2, 180 40, Praha 8, Czech Republic
[m] Dipartimento di Fisica, Università di Genova and INFN, Via Dodecaneso 33, I-16146 Genova, Italy
[n] Institut des Sciences Nucléaires, IN2P3-CNRS, Université de Grenoble 1, F-38026 Grenoble Cedex, France
[o] Helsinki Institute of Physics, HIP, P.O. Box 9, FIN-00014 Helsinki, Finland
[p] Joint Institute for Nuclear Research, Dubna, Head Post Office, P.O. Box 79, 101 000 Moscow, Russian Federation
[q] Institut für Experimentelle Kernphysik, Universität Karlsruhe, Postfach 6980, D-76128 Karlsruhe, Germany
[r] Institute of Nuclear Physics and University of Mining and Metalurgy, Ul. Kawiory 26a, PL-30055 Krakow, Poland
[s] Université de Paris-Sud, Lab. de l'Accélérateur Linéaire, IN2P3-CNRS, Bât. 200, F-91405 Orsay Cedex, France
[t] School of Physics and Chemistry, University of Lancaster, Lancaster LA1 4YB, UK
[u] LIP, IST, FCUL - Av. Elias Garcia, 14-1(o), P-1000 Lisboa Codex, Portugal
[v] Department of Physics, University of Liverpool, P.O. Box 147, Liverpool L69 3BX, UK
[w] LPNHE, IN2P3-CNRS, Universités Paris VI et VII, Tour 33 (RdC), 4 place Jussieu, F-75252 Paris Cedex 05, France
[x] Department of Physics, University of Lund, Sölvegatan 14, S-22363 Lund, Sweden
[y] Université Claude Bernard de Lyon, IPNL, IN2P3-CNRS, F-69622 Villeurbanne Cedex, France
[z] Univ. d'Aix - Marseille II - CPP, IN2P3-CNRS, F-13288 Marseille Cedex 09, France
[aa] Dipartimento di Fisica, Università di Milano and INFN, Via Celoria 16, I-20133 Milan, Italy
[ab] Niels Bohr Institute, Blegdamsvej 17, DK-2100 Copenhagen 0, Denmark
[ac] NC, Nuclear Centre of MFF, Charles University, Areal MFF, V Holesovickach 2, 180 00, Praha 8, Czech Republic
[ad] NIKHEF, Postbus 41882, NL-1009 DB Amsterdam, The Netherlands
[ae] National Technical University, Physics Department, Zografou Campus, GR-15773 Athens, Greece
[af] Physics Department, University of Oslo, Blindern, N-1000 Oslo 3, Norway
[ag] Dpto. Fisica, Univ. Oviedo, Avda. Calvo Sotelo, S / N-33007 Oviedo, Spain, (CICYT-AEN96-1681)
[ah] Department of Physics, University of Oxford, Keble Road, Oxford OX1 3RH, UK
[ai] Dipartimento di Fisica, Università di Padova and INFN, Via Marzolo 8, I-35131 Padua, Italy
[aj] Rutherford Appleton Laboratory, Chilton, Didcot OX11 0QX, UK
[ak] Dipartimento di Fisica, Università di Roma II and INFN, Tor Vergata, I-00173 Rome, Italy
[al] CEA, DAPNIA / Service de Physique des Particules, CE-Saclay, F-91191 Gif-sur-Yvette Cedex, France
[am] Istituto Superiore di Sanità, Ist. Naz. di Fisica Nucl. (INFN), Viale Regina Elena 299, I-00161 Rome, Italy
[an] Instituto de Fisica de Cantabria (CSIC-UC), Avda. los Castros, S / N-39006 Santander, Spain, (CICYT-AEN96-1681)
[ao] Inst. for High Energy Physics, Serpukov P.O. Box 35, Protvino, (Moscow Region), Russian Federation
[ap] J. Stefan Institute, Jamova 39, SI-1000 Ljubljana, Slovenia
and Department of Astroparticle Physics, School of Environmental Sciences, Kostanjeviska 16a, Nova Gorica, SI-5000 Slovenia
and Department of Physics, University of Ljubljana, SI-1000 Ljubljana, Slovenia
[aq] Fysikum, Stockholm University, Box 6730, S-113 85 Stockholm, Sweden

[ar] Dipartimento di Fisica Sperimentale, Università di Torino and INFN, Via P. Giuria 1, I-10125 Turin, Italy

[as] Dipartimento di Fisica, Università di Trieste and INFN, Via A. Valerio 2, I-34127 Trieste, Italy
and Istituto di Fisica, Università di Udine, I-33100 Udine, Italy

[at] Univ. Federal do Rio de Janeiro, C.P. 68528 Cidade Univ., Ilha do Fundão BR-21945-970 Rio de Janeiro, Brazil

[au] Department of Radiation Sciences, University of Uppsala, P.O. Box 535, S-751 21 Uppsala, Sweden

[av] IFIC, Valencia-CSIC, and D.F.A.M.N., U. de Valencia, Avda. Dr. Moliner 50, E-46100 Burjassot (Valencia), Spain

[aw] Institut für Hochenergiephysik, Österr. Akad. d. Wissensch., Nikolsdorfergasse 18, A-1050 Vienna, Austria

[ax] Inst. Nuclear Studies and University of Warsaw, Ul. Hoza 69, PL-00681 Warsaw, Poland

[ay] Fachbereich Physik, University of Wuppertal, Postfach 100 127, D-42097 Wuppertal, Germany

Abstract

Oscillations of B_s^0 mesons were studied in events with a large transverse momentum lepton selected from 3.2 million hadronic Z^0 decays registered by DELPHI between 1991 and 1994. A limit on the mass difference between the physical B_s^0 states

$$\Delta m_s > 6.5 \, \text{ps}^{-1} \text{ at } 95\% \text{ C.L.}$$

was obtained by combining the results obtained in three channels. © 1997 Published by Elsevier Science B.V.

1. Introduction

In the Standard Model, B_q^0–$\overline{B_q^0}$ (q = d,s) mixing is a direct consequence of second order weak interactions. Starting with a B_q^0 meson produced at time $t = 0$, the probability, $\mathcal{P}$, to observe a B_q^0 decaying at the proper time t can be written, neglecting effects from CP violation:

$$\mathcal{P}\left(B_q^0 \to B_q^0\right) = \frac{\Gamma_q}{2} e^{-\Gamma_q t}$$

$$\times \left[\cosh\left(\frac{\Delta\Gamma_q}{2} t\right) + \cos(\Delta m_q t)\right].$$

Here $\Gamma_q = \frac{\Gamma_q^H + \Gamma_q^L}{2}$, $\Delta\Gamma_q = \Gamma_q^H - \Gamma_q^L$, and $\Delta m_q = m_q^H - m_q^L$, where H and L denote respectively the heavy and light physical states. The oscillation period gives a direct measurement of the mass difference between the two physical states. The Standard Model predicts that $\Delta\Gamma \ll \Delta m$. Neglecting a possible difference between the B_s^0 lifetimes of the heavy and light eigenstates, which could be between 10 to

20% [1], and writing $\tau_q = 1/\Gamma_q$, the above expression simplifies to:

$$\mathcal{P}_{B_q^0}^{\text{unmix}} = \mathcal{P}\left(B_q^0 \to B_q^0\right)$$

$$= \frac{1}{2\tau_q} e^{-\frac{t}{\tau_q}} \left[1 + \cos(\Delta m_q t)\right]$$

and similarly:

$$\mathcal{P}_{B_q^0}^{\text{mix}} = \mathcal{P}\left(B_q^0 \to \overline{B_q^0}\right) = \frac{1}{2\tau_q} e^{-\frac{t}{\tau_q}} \left[1 - \cos(\Delta m_q t)\right]$$

At LEP any mixing measurements are sensitive to B_d^0 and B_s^0 meson oscillations. The time integrated mixing probability has already been measured [2]. It is defined as $\overline{\chi} = P_d \chi_d + P_s \chi_s$ where the P_q are the B_q^0 fractions in b jets, and the $\chi_q = x_q^2/2(1 + x_q^2)$, with $x_q = \Delta m_q/\Gamma_q$, are the time integrated mixing probabilities for the B_q^0 mesons. The parameter χ_d has already been measured at the $\Upsilon(4S)$ [3] and Δm_d at LEP, where time dependent oscillations of B_d^0 mesons were measured and limits on Δm_s obtained [4,5].

The results presented here were obtained from data registered by DELPHI between 1991 and 1994 (1995 data were also analysed for the $(\ell, D_s) - Q_{hem}$ analysis). The principle of these measurements was as follows. Each of the charged and neutral particles measured in an event was assigned to one of the two hemispheres defined by the plane transverse to the sphericity axis. In one hemisphere, a "production tag" was then defined which is correlated to the $b/\bar{b}$ sign of the initial quark at the production point; in the other hemisphere, the decay time of the B hadron was evaluated and a "decay tag" was defined, correlated with the $B/\bar{B}$ nature of the decaying hadron.

Three analyses were performed using events containing a lepton emitted at large transverse momentum, p_t, relative to its jet axis. The lepton charge defines the "decay tag". In two of these analyses the "production tag" was obtained from the value of the hemisphere charge measured in the hemisphere opposite to the lepton (Q_{hem}): they will be called the $\ell - Q_{hem}$ channel and the $(D_s\ell) - Q_{hem}$ channel. In the latter, the identified lepton is accompanied by an exclusively reconstructed D_s in the same hemisphere. The third channel, $\ell - \ell$, uses events with two high p_t leptons, identified in opposite hemispheres, and it is not possible to separate the notions of "decay" and "production" tags.

Sections 2 and 3 describe the main features of the DELPHI detector and the event selection and simulation. Section 4 presents the algorithm used for the hemisphere charge reconstruction. Section 5 explains the procedure used to set limits on Δm_s. Sections 6 to 8 present the different analyses. The combined result is given in Section 9.

2. The DELPHI detector

The events used in this analysis were recorded with the DELPHI detector at LEP running near the Z^0 peak. The performance of the detector is described in [6]. The relevant parts for lepton identification are the muon chambers and the electromagnetic calorimeters. The Vertex Detector (VD) is used in combination with the central tracking devices to measure precisely the charged particle trajectories close to the beam interaction region.

The DELPHI reference frame is defined with z along the e^- beam, x towards the centre of LEP, and y upwards. The angular coordinates are the polar angle θ, measured from the z axis, and the azimuth angle ϕ, measured from the x-axis. R is the radial distance from the z-axis.

The muon chambers are drift chambers located at the periphery of DELPHI. The barrel part ($-0.63 < \cos\theta < 0.63$) is composed of three sets of modules, each of two active layers, that give z and $R\phi$ coordinates. In the forward part, two layers of two planes give the x and y coordinates in the transverse plane. The precision of these detectors has to be taken into account for muon identification: it was measured to be 1 cm in z and 0.2 cm in $R\phi$ for the barrel part, and 0.4 cm for each of the two coordinates given by the forward part. The number of absorption lengths in front of the muon chambers, which largely determines the hadron contamination, is approximately 8 for $\theta = 90°$.

Electrons are absorbed in the electromagnetic calorimeters. The High density Projection Chamber (HPC), which covers the angular region used in this analysis, provides three dimensional information on electromagnetic showers. It has 18 radiation lengths thickness for $\theta = 90°$.

During the first part of the data taking period (1991 to 1993), the Vertex Detector [7] consisted of three concentric shells of silicon strip detectors, at average radii of 6.3, 9 and 11 cm, that measured the coordinates of charged particle tracks in the transverse plane with respect to the beam direction ($R\phi$) with a precision of 8 μm. The association of this detector with the central tracking system of DELPHI, consisting of the Time Projection Chamber (TPC) and the Inner and Outer Detectors, gave a precision of $\sqrt{20^2 + (65/p)^2}$ μm (with p in GeV/c) on the transverse impact parameter of charged particles with respect to the primary vertex. For the data registered in 1994, the inner and outer shells of the VD were equipped with double-sided detectors, providing in addition an accurate measurement of the charged particle trajectories along the beam direction (z). The single hit precision of the z coordinate is a function of the incident angle of the track, reaching a value of 9 μm for tracks perpendicular to the modules.

The 192 sense wires of the TPC measure the

specific energy loss, dE/dx, of charged particles as the 80% truncated mean of the amplitudes of the wire signals with a minimum requirement of 30 wires. This dE/dx measurement is available for 75% of charged particles in hadronic jets, with a precision which was measured to be 6.7% in the momentum range $4 < p < 25$ GeV/c. It was used in electron identification.

To identify kaons with momenta between 3 and 15 GeV/c (this range corresponds to the typical momentum for kaons from a B decay), the gas radiator of the barrel Ring Imaging CHerenkov detector (RICH) [8] was used: below 8.5 GeV/c, it works in the *veto* mode (kaons and protons give no Cherenkov photons and were thus distinguished from pions and leptons, but not from each other); above this threshold, kaons were distinguished from all other charged particles by measuring the radius of the ring of detected Cherenkov photons.

3. Event selection and simulation

Hadronic decays of the Z^0 were selected by requiring the total energy of the charged particles in each hemisphere to exceed 3 GeV (assuming all charged particles to be pions), the total energy of the charged particles to exceed 15 GeV, and at least 5 charged particles with momenta above 0.2 GeV/c.

Each selected event was divided into two hemispheres separated by the plane transverse to the sphericity axis. A clustering analysis based on the JETSET algorithm LUCLUS [9] with default parameters was used to define jets, using both charged and neutral particles. These jets were used to compute the p_t^{out} of each particle in the event, defined as its momentum transverse to the axis of the rest of the jet it belongs to, after removing the particle itself.

Simulated events were generated using the JETSET 7.3 program [9] with parameters tuned as in [10] and an updated description of B decays. B hadron semileptonic decays were simulated using the ISGW model [11]. The generated events were followed through the full simulation of the DELPHI detector (DELSIM) [6], and the resulting simulated raw data were processed through the same reconstruction and analysis programs as the real data.

4. b / b̄ tagging using the mean hemisphere charge

The mean charge of an event hemisphere is defined as:

$$Q_{\text{hem}} = \frac{\sum\limits_{i=1}^{n} q_i (p_i \cdot e_s)^\kappa}{\sum\limits_{i=1}^{n} (p_i \cdot e_s)^\kappa} \qquad (1)$$

where q_i and p_i are the charge and the momentum of particle i, e_s is the unit vector along the sphericity axis, and $\kappa = 0.6$. The sum is extended over all charged particles present in the hemisphere. The value chosen for κ corresponds to the best separation between the Q_{hem} distributions for $b/\bar{b}$ quarks, according to the simulation.

In the $\ell - Q_{\text{hem}}$ channel, only the mean charge of the hemisphere opposite to the lepton, $Q_{\text{hem}}^{\text{oppo}}$, was used. For pure $b\bar{b}$ events, if a $\bar{b}$ candidate was selected by requiring $Q_{\text{hem}}^{\text{oppo}} > 0.0$, the fraction of correct tags, ϵ_b^{tag}, in the simulation is $(64.2 \pm 0.2)\%$. If ϵ is the fraction of the original b events remaining in the tagged sample, the statistical significance of a signal from oscillations is proportional to $\sqrt{\epsilon}(2\epsilon_b^{\text{tag}} - 1)$. The statistical significance was found to be optimised by requiring $|Q_{\text{hem}}^{\text{oppo}}| > 0.10$, giving $\epsilon_b^{\text{tag}} = (68.8 \pm 0.2)\%$ and an efficiency of 67.5% in the simulation. In the study of $B_d^0 - \overline{B_d^0}$ oscillations using the same data sample [5], the purity of precisely this tagging was measured directly from the data; a lower value was obtained, $\epsilon_b^{\text{tag}} = (67.3 \pm 0.5)\%$. This value obtained from the data was used in the present analysis.

In the $(D_s \ell) - Q_{\text{hem}}$ channel, the mean charge of the hemisphere containing the $D_s \ell$ system was also used, after excluding all the charged particles coming from the B_s^0 decay, i.e. the lepton and the D_s decay products:

$$Q_{\text{tot}} = Q_{\text{hem}}^{\text{oppo}} - Q_{\text{hem}}^{\text{same}} (\text{except } D_s, \ell) \qquad (2)$$

This results in using only particles from fragmentation, which carry information only about the original $b/\bar{b}$ quark charge as they are not affected by the oscillation of the neutral B^0 mesons. In the simulation, this improves the fraction of correct tags, ϵ_b^{tag}, from $(64.2 \pm 0.2)\%$ to $(70.5 \pm 0.5)\%$ while retaining

100% efficiency. To take into account the 1.5% difference between the tagging efficiencies in data and simulation observed in the $\ell - Q_{\text{hem}}$ channel (see above), a conservative value of $\epsilon_b^{\text{tag}} = (69.0 \pm 2.0)\%$ was used in the analysis.

In the analysis of B-$\overline{\text{B}}$ oscillations, the probabilities of classifying non-$b\bar{b}$ events as mixed or unmixed candidates must also be evaluated. As these events are a small fraction of the selected sample, the corresponding values were obtained from the simulation. Conservative uncertainties on these quantities were used when evaluating their contributions to systematic errors.

5. Procedure used to set a limit on Δm_s

Limits on Δm_s were obtained using the "amplitude" method [12]. In this method, an oscillation amplitude, A, is fitted for each assumed value of Δm_s. The equations for $\mathscr{P}_{\text{B}_s^0}^{\text{mix}}$ and $\mathscr{P}_{\text{B}_s^0}^{\text{unmix}}$ become:

$$\mathscr{P}_{\text{B}_s^0}^{\text{unmix}} = \mathscr{P}\left(\text{B}_s^0 \to \text{B}_s^0\right)$$
$$= \frac{1}{2\tau_s} e^{-\frac{t}{\tau_s}} \left[1 + A\cos(\Delta m_s t)\right] \qquad (3)$$

and

$$\mathscr{P}_{\text{B}_s^0}^{\text{mix}} = \mathscr{P}\left(\text{B}_s^0 \to \overline{\text{B}_s^0}\right)$$
$$= \frac{1}{2\tau_s} e^{-\frac{t}{\tau_s}} \left[1 - A\cos(\Delta m_s t)\right] \qquad (4)$$

For $A = 1$, the standard time distribution expressions for mixed and unmixed candidates given in Section 1 are recovered. In the limit of infinite statistics, the value of $A(\Delta m_s)$ can lie between 1 (for the true Δm_s value) and 0 (far from the true Δm_s value); in fact $A(\Delta m_s)$ is the Fourier transform of the observed proper time distribution of the mixed (Eq. (4)) or unmixed (Eq. (3)) decays, extracted taking experimental resolutions and efficiencies into account, and normalised to have a unit expected peak amplitude. Its expected form is approximately a Breit-Wigner [12]

$$A(\Delta m_s) = \frac{F(\Delta m_s)}{F(\Delta m_s^{\text{true}})}$$
$$\times \frac{\Gamma^2}{\left[\Gamma^2 + \left(\Delta m_s^{\text{true}} - \Delta m_s\right)^2\right]} \qquad (5)$$

where the factor $F(\Delta m_s)/F(\Delta m_s^{\text{true}})$ absorbs damping terms due to sample purity, mis-tagging and resolution that reduce the size of the oscillation expected for given Δm_s, and the width Γ reflects the limited effective proper time range of the measurement due to the B_s^0 lifetime and to the degradation of the proper time resolution with increasing proper time.

Compared with the likelihood approach, in the amplitude approach it is easier a priori:

· to add contributions from systematic uncertainties,

· to see the effect of large statistical fluctuations or systematic bias,

· to combine different channels and/or experiments,

and the amplitude approach has therefore been adopted by the LEP Oscillations Working Group [13].

Each measurement of A at a given value of Δm_s, A_m, is described by a Gaussian probability density function, $G(A, A_m, \sigma_{A_m})$, centred at $A = A_m$ where σ_{A_m} is the error on the measured amplitude. Several procedures can be used to set a limit in this situation, as described by the PDG [14]. The best procedure to apply for Δm_s has not yet been agreed.

Two of these procedures are:

· A given value of Δm_s is excluded with 95% C.L. when, if this value were the correct one, the probability of observing an amplitude value lower than the observed one would be below 5%. This corresponds to $\int_1^\infty G(A, A_m, \sigma_{A_m}) dA < 0.05$, and in the case of a Gaussian distribution to

$$A_m < 1 - 1.645\sigma_{A_m} \qquad (6)$$

This method gives a true 95% C.L. limit, in the sense that the true value of Δm_s will be 'excluded' in 5% of measurements. It has the undesirable property, however, that even a very high true Δm_s value that is in fact undetectable given the experimental resolution will be 'excluded', unrealistically, by a 'lucky' fluctuation, 5% of the time. If this method is used, the corresponding 'exclusion probability' discussed further below (or other equivalent information) should therefore also be quoted; its smallest possible value in this method is 5%, and values near 5% correspond to

completely unrealistic limits.

· The same procedure as in a), but limited to positive amplitudes:

$$\frac{\int_1^\infty G(A,A_m,\sigma_{A_m})dA}{\int_0^\infty G(A,A_m,\sigma_{A_m})dA} < 0.05 \qquad (7)$$

This method completely eliminates unrealistic limits, at the cost of being excessively conservative in the Δm_s region where realistic limits are possible.

Following current practice [13], procedure (a) is used in this paper. We also give the corresponding exclusion probabilities; and the result of the second procedure (b) is also reported for comparison.

Systematic uncertainties were evaluated by varying, according to their respective uncertainties, the values of the input parameters which were kept constant in the evaluation of the log-likelihood function. For each input parameter (q), the variation of the amplitude and of its measurement error were both taken into account in the evaluation of the systematic uncertainty.

This was done in the following way. If $f(q)$ is the probability distribution for the input parameter q, the confidence level that the fitted amplitude will not exceed unity is:

$$CL = \int_{-\infty}^{+\infty} f(q)$$
$$\times \int_1^{+\infty} G(A,A_m(q),\sigma_{A_m}(q))dA\,dq \qquad (8)$$

This expression was evaluated for each parameter, assuming that $f(q)$ is a Gaussian centred on q_0 and of variance σ_{q_0}, and using the values of $A_m(q)$ and $\sigma_{A_m}(q)$ fitted for five values of q, namely q_0, $q_0 \pm 1.5\sigma_{q_0}$, and $q_0 \pm 3.0\sigma_{q_0}$. Thus the integral was approximated by the sum:

$$\overline{CL} = \frac{\sum_{i=1}^5 f(q_i) \int_1^{+\infty} G(A,A_m(q_i),\sigma_{A_m}(q_i))\,dA}{\sum_{i=1}^5 f(q_i)} \qquad (9)$$

From the values of $\overline{CL}$ and of the amplitude $A(q_0)$, an effective variance $\overline{\sigma_A^2(q_0)}$ was evaluated. This

was then interpreted as resulting from the statistical error $\sigma_A(q_0)$ and an additional systematic uncertainty $\sigma_A(q_0)(\text{syst})$, determined from

$$\sigma_A^2(q_0)(\text{syst}) = \overline{\sigma_A^2(q_0)} - \sigma_A^2(q_0) \qquad (10)$$

Using five values of q in this way gives an accuracy of the order of 5% on the systematic uncertainty.

In the amplitude approach, it is also easy to compute the exclusion probability $\mathscr{P}_{\text{limit}}$, i.e. the probability of obtaining a 95% C.L. limit at a given value of Δm_s using the channel studied. It has to be assumed that the real value of Δm_s is much larger than the Δm_s value considered, so that the expected value of the amplitude is equal to zero. According to Eq. (6), all measured values of A which satisfy $A < 1 - 1.645\sigma_A$ are such that the corresponding value of Δm_s is excluded at 95% C.L. Then $\mathscr{P}_{\text{limit}}$ can be written as:

$$\mathscr{P}_{\text{limit}} = 1 - \int_{1-1.645\sigma_A}^\infty G(A,0,\sigma_A)\,dA \qquad (11)$$

6. The $(D_s^\pm \ell^\mp - Q_{\text{hem}})$ analysis

In this analysis, $B_s^0 - \overline{B_s^0}$ oscillations were measured using an exclusively reconstructed D_s meson correlated with a lepton of opposite charge emitted in the same hemisphere:

$$\overline{B_s^0} \to D_s^+ \ell^- \bar{\nu} X.$$

D_s mesons were identified in five non-leptonic and two semileptonic decay modes:

$D_s^+ \to \phi\pi^+$	$\phi \to K^+K^-$;
$D_s^+ \to \overline{K}^{\star 0}K^+$	$\overline{K}^{\star 0} \to K^-\pi^+$;
$D_s^+ \to K_S^0 K^+$	$K_S^0 \to \pi^+\pi^-$;
$D_s^+ \to f_0(980)\pi^+$	$f_0(980) \to \pi^+\pi^-$;
$D_s^+ \to \overline{K}^{\star 0}K^{\star +}$	$\overline{K}^{\star 0} \to K^-\pi^+, K^{\star +} \to K_S^0\pi^+$;
$D_s^+ \to \phi e^+\nu_e$	$\phi \to K^+K^-$;
$D_s^+ \to \phi\mu^+\nu_\mu$	$\phi \to K^+K^-$.

6.1. D_s non-leptonic decay modes

D_s^+ candidates were selected using the procedures described in [15] for the first three channels. For the

two remaining non-leptonic channels the selection is described below.

6.1.1. $D_s^+ \to f_0(980)\pi^+$

$D_s^+ \to f_0(980)\pi^+$ candidates were reconstructed by making all possible combinations of three charged particles in the same hemisphere that were geometrically compatible, i.e. had a vertex fit probability greater than 5%.

The following kinematic cuts were applied:
- at least one of the particles had $p > 1.5$ GeV/c,
- each particle had an energy loss measured in the TPC compatible within 3σ with the pion hypothesis,
- each had at least one associated hit in the silicon vertex detector (VD),
- $|M(\pi^+\pi^-) - M_{\mathrm{PDG}}(f_0(980))| < 100$ MeV/c^2,
- $p(D_s^+) > 10$ GeV/c.

where p is the momentum, M is the reconstructed mass, and the suffix PDG indicates the world average value [14].

Further background reduction was achieved by requiring the probability for the track impact parameters relative to the beam interaction position, in the hemisphere opposite to the one containing the D_s candidate, to be incompatible with that expected for lighter quark events [16] (i.e. by requiring probability < 0.001).

6.1.2. $D_s^+ \to \overline{K}{\star}0 K^{\star+}$

$D_s^+ \to \overline{K}{\star}0 K^{\star+}$ candidates were selected by reconstructing $K_S^0 \to \pi^+\pi^-$ decays accompanied in the same hemisphere by two charged tracks of the same electric charge and by a "loosely" identified kaon [6] of opposite electric charge (in the following, the categories "tight", "standard" and "loose" as defined in [6] will be used).

K_S^0 candidates were obtained by combining all pairs of tracks of opposite electric charge, and applying the "tight" selection criteria described in [6]. The K_S^0 trajectory and the remaining three tracks were tested for geometrical compatibility with a single vertex by requiring $\chi^2(D_s\,\mathrm{vertex}) < 20$. Since the track parameters of the K_S^0 had large measurement errors, at least one VD hit associated to each of the other three charged tracks was required in order to improve the vertex resolution. To reduce the

combinatorial background, the following kinematic cuts were also applied:
- $p(\pi^+) > 0.5$ GeV/c for both pions,
- $p(K^-) > 1$ GeV/c,
- $|M(K^-\pi^+) - M_{\mathrm{PDG}}(\overline{K}{\star}0)| < 50$ MeV/c^2,
- $|M(K_S^0\pi^+) - M_{\mathrm{PDG}}(K^{\star+})| < 50$ MeV/c^2,
- $p(D_s) > 9$ GeV/c.

6.1.3. Further treatment of non-leptonic decays

In all non-leptonic modes, the measured position of the D_s^+ decay vertex, the D_s^+ momentum, and their measurement errors, were used to reconstruct a D_s^+ particle. A candidate B_s^0 decay vertex was obtained by intercepting this particle with a "loosely" identified lepton [6] (electron or muon) of opposite charge in the same hemisphere (as for hadron identification, leptons were also classified as "tight", "standard" and "loose"). The lepton was required to have a high momentum ($p > 3$ GeV/c) and high transverse momentum ($p_t^{\mathrm{out}} > 1.1$ GeV/c) to suppress fake leptons and cascade decays ($b \to c \to \ell^+$) of non-strange B hadrons; the lepton track had also to be associated to at least one hit in the VD.

Further cascade background suppression was achieved by applying a cut on the probability that all the tracks accompanying the $D_s^\pm\ell^\mp$ system in the same hemisphere come from the primary vertex [16]. In addition, the following kinematic cuts were applied:
- $3.0 < M(D_s^\pm\ell^\mp) < 5.5$ GeV/c^2,
- $p(D_s^\pm\ell^\mp) > 14$ GeV/c,
- $\chi^2(B_s^0\,\mathrm{vertex}) < 20$.

In the D_s^+ mass region, a clear excess of "right-sign" combinations ($D_s^\pm\ell^\mp$) over "wrong-sign" combinations ($D_s^\pm\ell^\pm$) was observed in each channel (Fig. 1). Table 1 gives the measured number of events (background subtracted) in the D_s^+ signal and the ratio of the combinatorial background events to the total. The mass distribution for non-leptonic decays was fitted using two Gaussian distributions of equal widths to account for the D_s and D^+ signals and an exponential for the combinatorial background. The D^+ mass was fixed to the nominal value of 1.869 GeV/c^2[14]. The overall mass distribution for all the non-leptonic decays is shown in (Fig. 2a). The fit yielded a signal of 128 ± 15 D_s decays in "right-sign" combinations, centred at a
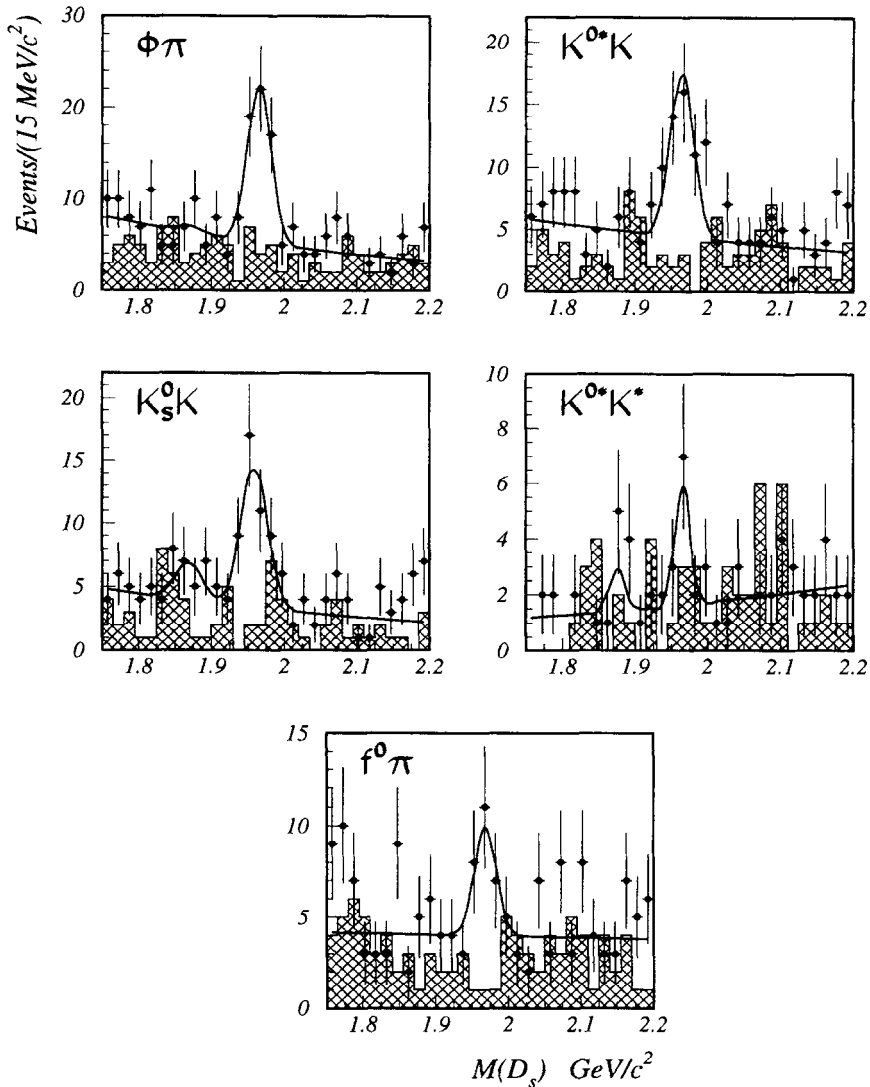
Fig. 1. $D_s^\pm \ell^\mp$ analysis: Invariant mass distributions for D_s candidates accompanied by a lepton of opposite electric charge identified in the same hemisphere and with p_t^{out} above 1.1 GeV/c. Five non-leptonic decay modes of the D_s were used. The wrong-sign combinations are given by the *shaded histograms*. The *curves* show the fits described in the text.

mass of 1.965 ± 0.002 GeV/c^2 with a width of 16 ± 2 MeV/c^2.

6.2. D_s semileptonic decay modes

The $(D_s^\pm \ell^\mp)$ candidates with D_s mesons decaying in the last two decay modes ($D_s^+ \rightarrow \phi \ell^+ \nu$, where $\ell = e$ or μ) were found by searching for $\phi \ell^+ \ell^-$ combinations in the same hemisphere.

The ϕ mesons were selected using the same kinematic cuts as in the $\phi \pi^+$ decay mode, but the identification cuts were tightened by requiring a loose identification for at least one of the two kaons from the ϕ.

Each lepton, "loosely" identified, was assigned to the D_s (B_s^0) if the mass of the $\phi \ell$ system, $M(\phi \ell)$, was below (above) the nominal D_s mass. If both leptons give a $M(\phi \ell)$ above or below the D_s

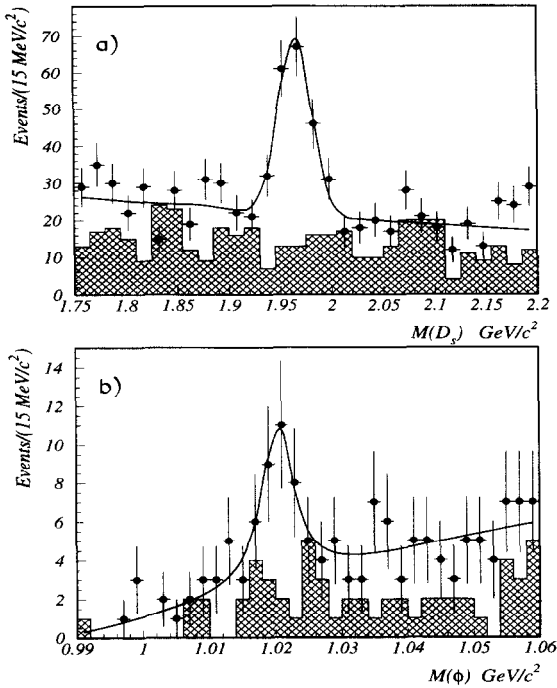Fig. 2. $D_s^{\pm} \ell^{\mp}$ analysis: a) The sum of the D_s^+ signals given in Figure 1. b) The $K^+ K^-$ invariant mass distribution for D_s candidates selected in the two semileptonic decay modes and accompanied by a lepton of opposite electric charge present in the same hemisphere having $p_t^{out} > 1.1\,\mathrm{GeV}/c$. Wrong-sign combinations ($D_s^{\pm} \ell^{\pm}$) are given by the *shaded histograms*. The *curves* show the fits described in the text.

mass the event was rejected. The following additional requirements were then applied:

- $p(\ell_{B_s^0}) > 3$ GeV/c, $p(\ell_{D_s}) > 1$ GeV/c,
- $p_t^{out}(\ell_{B_s^0}) > 1.2$ GeV/c,
- $\chi^2_{D_s\,\mathrm{vertex}} < 50$, $\chi^2_{B_s^0\,\mathrm{vertex}} < 30$,
- 2.5 GeV/c$^2 < M(\phi\ell\ell) < 5.5$ GeV/c^2.

As in the previous analysis, the *b*-tagging probability, in the hemisphere opposite to the one containing the D_s candidate was required to be compatible with that expected for a *b* event. Further background reduction was achieved by requiring a missing energy, E_{miss}, correlated with a lepton momentum, $p(\ell_{B_s^0})$, in the same hemisphere satisfying:

$$\sqrt{\left(E_{\mathrm{miss}}/10\right)^2 + \left(p(\ell_{B_s^0})/5\right)^2} > 1\,\mathrm{GeV}$$

where E_{miss} was defined as:

$$E_{\mathrm{miss}} = E_{\mathrm{tot}} - E_{\mathrm{vis}}$$

where the visible energy (E_{vis}) is the sum of the energies of charged particles and photons in the same hemisphere as the $D_s\ell$ candidate and, using four-momentum conservation, the total energy (E_{tot}) in that hemisphere is:

$$E_{\mathrm{tot}} = E_{\mathrm{beam}} + \frac{M_{\mathrm{same}}^2 - M_{\mathrm{opp}}^2}{4E_{\mathrm{beam}}}$$

where M_{same} and M_{opp} are the hemisphere invariant masses of the same and opposite hemispheres respectively.

The selected events showed a clear excess of "right-sign" with respect to "wrong-sign" combinations (Fig. 2b). The $K^+ K^-$ invariant mass distribution for "right sign" events was fitted with a Breit–Wigner distribution to account for the signal, and a polynomial function to describe the combinatorial background. The fit gave 38 ± 11 events (see Table 1) centred at a mass of 1.020 ± 0.001 GeV/c^2 with a total width of 6 ± 2 MeV/c^2.

6.3. Sample composition

B_s^0 meson oscillations were studied using events in the right-sign sample lying in a mass interval of $\pm 2\sigma$ ($\pm 1\Gamma$) centred on the measured D_s (ϕ) mass.

The following components in the selected event sample were considered [15]:

- f_{bkg} being the fraction of events from the combinatorial background. It was evaluated from the fit to the mass distribution of right-sign events and is given in Table 1.

Table 1
Numbers of D_s signal events and ratios of the combinatorial background events to the total in the D_s decay channels. The level of the combinatorial background was evaluated using a mass interval of $\pm 2\sigma$ ($\pm 1\Gamma$) centred on the measured D_s (ϕ) mass.

D_s decay modes	Estimated signal	Combinatorial background
		Total
$D_s \to \phi\pi^+$	45 ± 8	0.33 ± 0.05
$D_s \to \overline{K}^{*0} K^+$	36 ± 7	0.35 ± 0.06
$D_s \to K_S^0 K^+$	35 ± 7	0.33 ± 0.06
$D_s \to \overline{K}^{*0} K^{*+}$	7 ± 3	0.36 ± 0.14
$D_s \to f_0(980)\pi^+$	16 ± 5	0.50 ± 0.12
$D_s \to \phi\ell^+\nu$	38 ± 11	0.38 ± 0.06

Table 2
Time resolution for different D_s decay modes parametrized using the sum of two Gaussian distributions. The width of the wider Gaussian was independent of the proper time whereas the width of the narrower depends on the generated proper time.

D_s decay mode	First Gaussian fraction (%)	First Gaussian resolution (ps)	Second Gaussian resolution (ps)
$K_S^0 K^+$ (91–93)	70	$0.157 + 0.038\ t$	0.9
$K_S^0 K^+$ (94–95)	80	$0.105 + 0.062\ t$	0.9
other non-leptonic (91–93)	80	$0.133 + 0.046\ t$	0.8
other non-leptonic (94–95)	80	$0.080 + 0.060\ t$	0.5
$\phi \ell^+ \nu$ (91–93)	80	$0.170 + 0.030\ t$	0.9
$\phi \ell^+ \nu$ (94–95)	80	$0.123 + 0.042\ t$	0.9

- f_{B_s} being the fraction of events in which D_s mesons are expected to come from B_s semileptonic decays.

- $f_{D_s D}$ being the expected fraction of cascade decays $B \to \overline{D}_{(\star)} D_s^{(\star)+} X$ followed by the semileptonic decay $\overline{D}_{(\star)} \to \ell^- \overline{\nu} X$ which gives right-sign $D_s^\pm \ell^\mp$ pairs. This source of background produces approximately the same number of events as the signal [15], but the selection efficiency is lower for cascade lepton events than for direct B semileptonic decays because of the requirement of a high p_t^{out} lepton and a high mass $(D_s \ell)$ system. After these cuts, the relative fractions are $f_{D_s D}/f_{B_s} = 0.106 \pm 0.020$ for non-leptonic decays and $f_{D_s D}/f_{B_s} = 0.102 \pm 0.022$ for semileptonic decays, as obtained from the simulation. The errors on these fractions result from the errors on the branching fractions of the processes contributing and the errors on the efficiency ratios.

- f_{refl} being the fraction of events from $D^+ \to K^- \pi^+ \pi^+$ and $D^+ \to K_S^0 \pi^+$ decays in which a π^+ was misidentified as a K^+ which give candidates in the D_s mass region. If the D^+ is accompanied by an oppositely charged lepton in the decay $\overline{B}_{u,d} \to D^+ \ell^- \overline{\nu} X$, it simulates a $\overline{B}_s^0$ semileptonic decay. The fractions $f_{refl}/f_{B_s} = 0.054 \pm 0.015$ and $f_{refl}/f_{B_s} = 0.069 \pm 0.025$ were obtained in the $\overline{K}_{\star 0} K^+$ and $K_S^0 K^+$ channels respectively.

6.4. Measurement of the B meson decay time

For each event, the B_s^0 proper decay time was obtained from the measured decay length (L_{B^0}) and

the estimate of the B_s^0 momentum $(p_{B_s^0})$. The B_s^0 momentum was estimated from:

$$p_{B_s^0}^2 = \left(E(D_s \ell) + E_\nu \right)^2 - m_{B_s^0}^2.$$

The neutrino energy E_ν was calculated from E_{miss} corrected by a function, deduced from the simulation, of the $(D_s \ell)$ energy [2]:

$$E_\nu = E_{miss} + F\left(E(D_s \ell) \right)$$

The details of this evaluation are given in [15].

Except for the combinatorial background contribution, the predicted proper time distributions were obtained by convoluting the theoretical functions with resolution functions evaluated from simulated events. Due to the different decay length resolutions, different proper time resolutions were considered for $K_S^0 K^+$ decays, for other non-leptonic decays, and for semileptonic D_s decays. Different time resolutions were also considered for the different Vertex Detector configurations in 91–93 and 94–95, respectively.

The proper time resolution was defined as the difference between the generated time (t) and the reconstructed time (t_i). The following proper time resolutions were considered:

- $\mathscr{R}_{B_s}(t - t_i)$ is the resolution function for signal events and for the mass reflection background. $\mathscr{R}_{B_s}$ was parametrized using two Gaussian distributions, the narrower one having a width varying

---

[2] here D_s means "observed decay products of D_s", including also the decays where the D_s is not fully reconstructed (specifically, $D_s \to \phi \ell \nu$)

linearly with the generated proper time. The values of the corresponding parameters are given in Table 2.

- $\mathscr{R}_{D_sD}(t - t_i)$ is the resolution function for the D_sD background. Since the measured proper time is overestimated for these events, $\mathscr{R}_{D_sD}(t - t_i)$ is
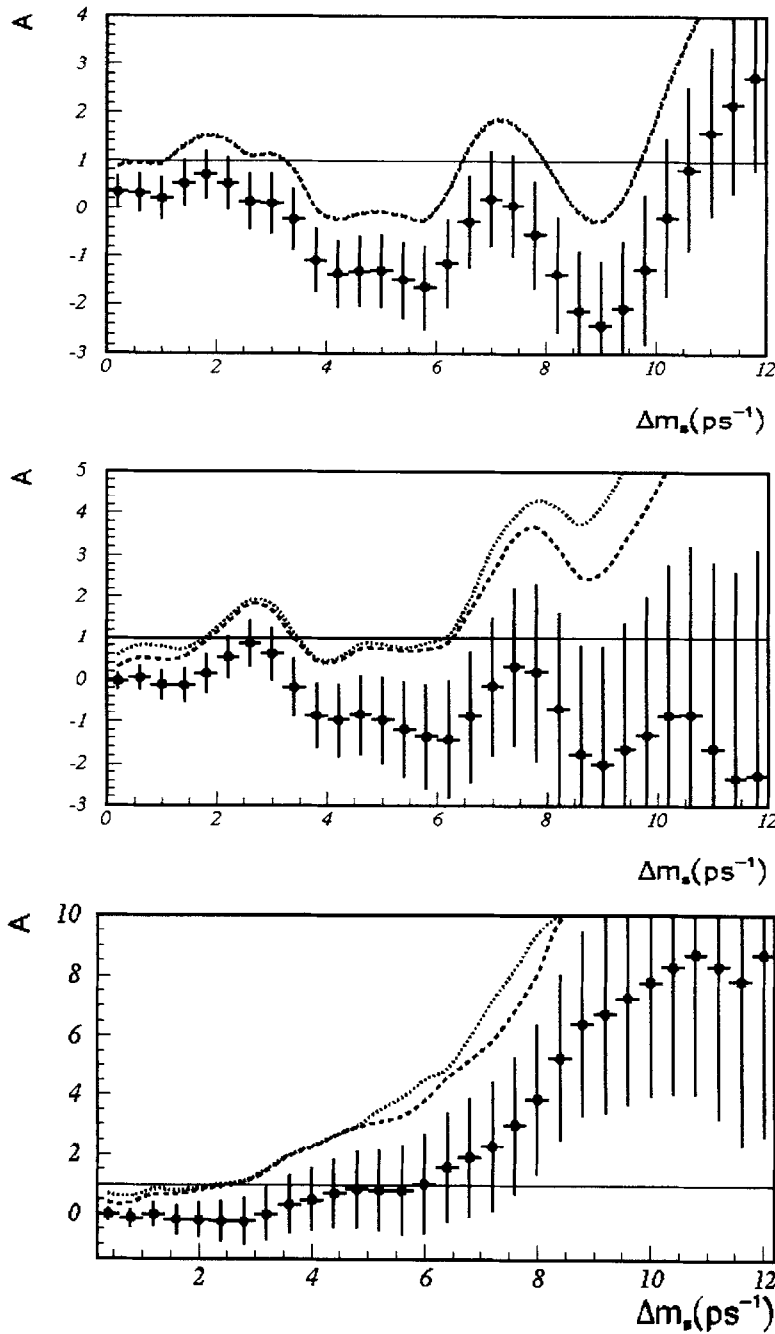

Fig. 3. Variation of the oscillation amplitude A as a function of Δm_s, from top to bottom for the $(D_s^{\pm}\ell^{\mp}) - Q_{hem}$, $\ell - Q_{hem}$ and $\ell - \ell$ analyses. The *dashed line* corresponds to $A + 1.645\sigma_A$ with statistical uncertainties only, while the *dotted line* includes the contribution from systematics.

well described by a Gaussian distribution convoluted with an exponential distribution. The dependence of the resolution on the generated proper time was neglected.

The time distribution $\mathscr{P}_{bkg}(t_i)$ for the combinatorial background was obtained directly from real data, by fitting the time distribution of wrong-sign and right-sign events situated in the wings of the D_s (ϕ) mass distribution.

6.5. Tagging procedure

An event was classified as a mixed or an unmixed candidate according to the sign of the D_s electric charge, Q_D, relative to the Q_{tot} variable (see Eq. (2)).

Mixed candidates were defined by requiring $Q_{tot} \times Q_D < 0$, and unmixed ones by requiring $Q_{tot} \times Q_D > 0$. The probability, ϵ_b^{tag}, of tagging the b or the $\bar{b}$ quark correctly from the measurement of Q_{tot} was evaluated as explained in Section 4. The corresponding probability for events in the combinatorial background was obtained using real data candidates selected in the wings of the signal: the probabilities of classifying these events as mixed or unmixed candidates are called ϵ_{bkg}^{mix} and ϵ_{bkg}^{unmix} respectively.

6.6. Fitting procedure.

Using the calculated proper time distributions and the tagging probabilities, the probability functions for mixed and unmixed events were computed [3]:

$$P^{mix}(t_i) = f_{B_s} P_{B_s}^{mix}(t_i) + f_{refl} P_{refl}^{mix}(t_i)$$
$$+ f_{D_sD} P_{D_sD}^{mix}(t_i)$$
$$+ f_{bkg} P_{bkg}^{mix}(t_i) \quad (12)$$

The analytical expressions for the different probability densities are as follows:
- B_s mixing probability.

$$P_{B_s}^{mix}(t_i)$$
$$= \left\{ \epsilon_b^{tag} \mathscr{P}_{B_s}^{mix}(t) + \left(1 - \epsilon_b^{tag}\right) \mathscr{P}_{B_s}^{unmix}(t) \right\} \quad (13)$$
$$\otimes \mathscr{R}_{B_s}(t - t_i)$$

- D_sD background mixing probability. Three contributions were considered, according to whether the D_sD events come from B_d^0 or B_s^0 mesons or from other B-hadrons. The first contribution has an oscillating component which depends on the values of Δm_d and τ_{B_d}. For the B_s^0 part, for each proper time equal contributions are expected from mixed and unmixed events, since either of the two D_s can decay semileptonically. The third sample contributes to the mixed events (because of the sign of the cascade lepton), and its time distribution is an exponential whose average is given by the mean B-hadron lifetime.

$$P_{D_sD}^{mix}(t_i) = \left\{ f_{B_d} \left(\epsilon_b^{tag} \mathscr{P}_{B_d}^{unmix}(t) \right. \right.$$
$$+ \left(1 - \epsilon_b^{tag}\right) \mathscr{P}_{B_d}^{mix}(t) \right)$$
$$+ \left(1 - f_{B_d} - f_{B_s}\right) \epsilon_b^{tag} \exp(-t/\tau_B)$$
$$\left. + \frac{f_{B_s}}{2} \exp\left(-t/\tau_{B_s}\right) \right\} \otimes \mathscr{R}_{D_sD}(t - t_i)$$
$$(14)$$

- Mass reflection background mixing probability. Since $D^{\pm}\ell^{\mp}$ events come mainly from B_d^0 decays, the following probability density was considered:

$$P_{refl.}^{mix}(t_i)$$
$$= f_{B_d} \left\{ \epsilon_b^{tag} \mathscr{P}_{B_d}^{mix}(t) + \left(1 - \epsilon_b^{tag}\right) \mathscr{P}_{B_d}^{unmix}(t) \right\}$$
$$\otimes \mathscr{R}_{B_s}(t - t_i)$$
$$(15)$$

- Combinatorial background mixing probability:

$$P_{bkg}^{mix}(t_i) = \epsilon_{bkg}^{mix} \mathscr{P}_{bkg}(t_i) \quad (16)$$

A negative log-likelihood function was then obtained. Using the amplitude approach (Fig. 3), and considering only the statistical uncertainties, the excluded regions of Δm_s are:

$$\Delta m_s < 1.0 \, \text{ps}^{-1}, \quad 3.2 < \Delta m_s < 6.5 \, \text{ps}^{-1},$$
$$8.0 < \Delta m_s < 9.7 \, \text{ps}^{-1} \text{ at } 95\% \text{ C.L.} \quad (17)$$

6.7. Study of systematic uncertainties

Systematic uncertainties were evaluated by varying the parameters which were kept constant in the fit according to their measured or expected errors.

---

[3] In the following, only the probability function for mixed events is written explicitly; the corresponding probability for unmixed events can be obtained by changing ϵ into $(1 - \epsilon)$.

- As explained in Section 4, the variable Q_{tot} was used. The tagging purity found in the simulation was (70.5 ± 0.5) % for 100 % efficiency. On the other hand, in the $\ell - Q_{hem}$ analysis [5], using only the tracks present in the hemisphere opposite to the lepton, the tagging purity fitted from the data was found to differ from the value measured in the simulation by $\epsilon_{jet}^{b}(\text{DATA}) - \epsilon_{jet}^{b}(\text{MC}) = -1.5 \pm 0.5\,(\text{stat}) \pm 1.5\%$. A conservative estimation of the tagging purity in the data is therefore $\epsilon_{jet}^{b} = (69.0 \pm 2.0)\%$.

- f_{bkg} was varied according to the statistical uncertainty of the fitted fraction of the combinatorial background present in the different D_s or K^+K^- mass distributions.

- If the errors are Gaussian, the oscillation amplitude is damped by a factor ρ because of the finite accuracy in the decay time σ_t:

$$\rho = e^{-(\Delta m_s \sigma_t)^2 / 2} \qquad (18)$$

where σ_t receives two contributions: one from decay distance errors and the other from momentum errors. At small decay times, the accuracy on t depends mainly on the resolution on the decay distance. This quantity was measured using the simulation, after having tuned the track reconstruction efficiencies and measurement errors to match the real data. For this purpose, tracks emitted at angles less than 30^0 from the horizontal plane were selected, so as benefit from the precise definition of the beam position in the vertical direction. The details of the tuning procedure are described in [16]. After the tuning, the agreement between real data and simulated data on the decay distance error was evaluated to be 10%. Using the algorithm described in [15], the B_s^0 momentum resolution was estimated to be 8%. To check the reliability of the B_s^0 momentum estimate, the distribution of the momentum estimated from the simulated signal events was compared with that from real data. The latter was obtained by subtracting the estimated momentum distribution of the combinatorial background, taken in the D_s side bands, from that of the events in the signal region. The results are reported in [15]. The systematic error coming from the uncertainties on the resolution functions was evaluated by varying by 10% the two parameters describing the linear
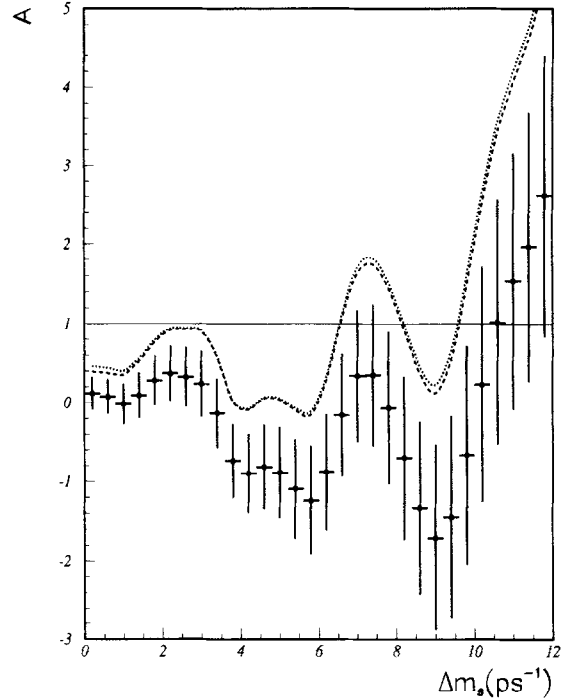

Fig. 4. Variation with Δm_s of the exclusion probability for each studied channel (upper plot) and for the combined result (lower plot).

time dependence of the narrower Gaussian (see Table 2). A variation of 10% of the resolution for the background events was also considered.

Including these systematic uncertainties does not change the excluded Δm_s regions significantly. The exclusion probability varies from 100% to 71% and from 47% to 28% for the two first regions, respectively. In the region $8.0 < \Delta m_s < 9.7\,\text{ps}^{-1}$, the exclusion probability varies between 22% and 18%. The variation of the exclusion probability as a function of Δm_s, obtained using the method described in Section 5, is given in Fig. 4.

7. The $\ell - Q_{hem}$ analysis

This analysis is very similar to that performed to extract a value of Δm_d in [5], which should be consulted for details. A lepton, of electric charge Q_ℓ, was identified in one hemisphere, and the mean charge of the opposite hemisphere was used to clas-

sify the events as mixed if $Q_{hem} \times Q_\ell > \Delta Q$ and as unmixed if $Q_{hem} \times Q_\ell < -\Delta Q$. As explained in Section 4, the value $\Delta Q = 0.10$ gives the best compromise between tagging efficiency and tagging purity. The numbers of events classified as mixed and unmixed were respectively 12988 and 19406 for the 1991–1993 data, and 11063 and 16924 in 1994.

Fig. 3 shows the fitted amplitude and its statistical errors. The following Δm_s intervals were excluded:

$$\Delta m_s < 1.9 \, \text{ps}^{-1}, \quad 3.3 < \Delta m_s < 6.3 \, \text{ps}^{-1}. \quad (19)$$

These limits correspond in (Fig. 3) to the crossing points of the line $A = 1$ with the continous line. Systematic uncertainties were evaluated by varying the parameters which had been kept constant in the fit according to their measured or expected errors. Values for these parameters are summarized in Table 3.

• The tagging purity ϵ_{jet}^b and Δm_d were measured, using the same data sample, in the study of B_d^0–$\overline{B_d^0}$ oscillations [5]. The respective variations of these parameters were applied, taking into account the measured correlation ($\rho = 0.62$) between their fitted uncertainties. Their effect is mainly important at low values of Δm_s.

• The fraction of B_s^0 mesons produced in a b quark jet was expressed in terms of the integrated oscillation rates, $\overline{\chi}$ and χ_d, and of the b-baryon production rate $P_{b\text{-baryons}}$:

$$P_s = \frac{2\overline{\chi} - \left(1 - P_{b\text{-baryons}}\right)\chi_d}{1 - \chi_d}. \quad (20)$$

In practice, the uncertainty on P_s depends mainly on the measurement errors on $\overline{\chi}$ and on χ_d, which were varied independently. Using the values reported in Table 3: $P_s = (10.2 \pm 2.0)\%$.

• The B_s^0 meson decay time was obtained from the measurements of the B meson decay distance and the B meson momentum. Details are given in [5]. In the simulation, the measured decay distance of each event was compared to the exact distance and the difference was varied by 10%. A similar procedure was applied for the measured momentum. The same procedure was applied for non-b events.

Including systematic uncertainties, the excluded regions of Δm_s become:

$$\Delta m_s < 1.7 \, \text{ps}^{-1},$$

$$3.4 < \Delta m_s < 6.1 \, \text{ps}^{-1} \text{ at 95\% C.L.} \quad (21)$$

These limits correspond in (Fig. 3) to the crossing points of the line $A = 1$ with the dashed line. The exclusion probability is 60% for 1.7 ps^{-1} and varies between 36% and 17% for the edges of the region corresponding to 3.4 and 6.1 ps^{-1} respectively. The variation of the exclusion probability as a function of Δm_s, obtained using the method described in Section 5, is shown in Fig. 4.

8. The ℓ–ℓ analysis

In this measurement, the decay sign was determined from the lepton in one hemisphere, provided a secondary vertex was reconstructed including that lepton, and the production sign was determined from the lepton in the opposite hemisphere. Details of this

Table 3
Central values and variations of the parameters considered in the study of systematic uncertainties.

Parameter	Central value and variation
tagging purity for $b - \overline{b}$ events	$\epsilon_{jet}^b = 0.673 \pm 0.005$ [5]
Δm_d	$\Delta m_d = 0.493 \pm 0.042 \, \text{ps}^{-1}$ [5]
integrated oscillation rate measured at LEP	$\overline{\chi} = 0.1217 \pm 0.0046$ [17]
integrated oscillation rate for B_d^0 mesons	$\chi_d = 0.174 \pm 0.016$ [14]
b-baryon fraction in b jets	$P_{b\text{-baryons}} = 0.087 \pm 0.029$ [14]
uncertainty on the control of the measurement of the B meson decay distance	$\pm 10\%$
uncertainty on the control of the measurement of the B meson momentum	$\pm 10\%$

analysis including the lepton selection criteria, the secondary vertex reconstruction and the expression for the likelihood function are described in [5].

An event was selected if there was at least one identified lepton per hemisphere and at least one reconstructed secondary vertex. It was classified as mixed if the charges of the two leptons were the same and as unmixed if they were different. The numbers of events classified as mixed and unmixed were 1579 and 3199 respectively.

Systematic uncertainties were again evaluated by varying, according to their respective uncertainties, the values of the parameters which were kept constant in the evaluation of the log-likelihood function. With respect to the parameters described in Section 7 and listed in Table 3, the variation of the tagging purity in jets was replaced by the variation of the fraction of wrong charge assignment, which was $\pm 6\%$. Fig. 3 gives the variation of the oscillation amplitude and of its error with Δm_s. The dashed line corresponds to the statistical error on the amplitude scaled by a factor 1.645. The dotted line includes the effect of systematic uncertainties. They affect the measurement at low values of Δm_s, and the control of the time resolution produces also significant effects at very high values of Δm_s.

Including systematic uncertainties in the measured amplitude, the 95% C.L. excluded region is

$$\Delta m_s < 2.8\,\text{ps}^{-1} \text{ at 95\% C.L.} \tag{22}$$

The exclusion probability for 2.8 ps^{-1} is 36%. The variation of the exclusion probability as a function of Δm_s, obtained using the method described in Section 5, is shown in Fig. 4.

9. Combined limit on Δm_s

The three analyses were combined, taking into account correlations between the event samples and between the systematic uncertainties in the different amplitude measurements (Fig. 5). This gave the result:

$$\Delta m_s > 6.5\,\text{ps}^{-1} \text{ at 95\% C.L.} \tag{23}$$

corresponding to $x_s > 10.5$, where $x_s = \Delta m_s / \Gamma_s = \Delta m_s \tau_{B_s^0}$ and $\tau_{B_s^0} = 1.61^{+0.10}_{-0.09}$ ps [14]. The exclusion probability for this limit is 36% (see Fig. 4). The
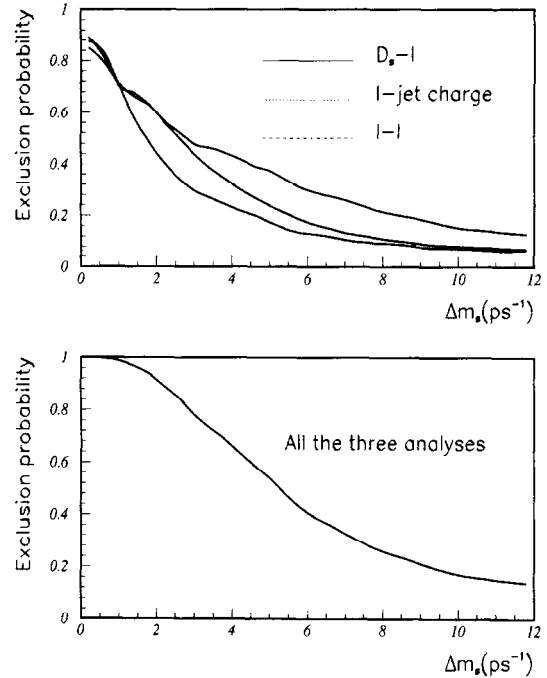

Fig. 5. Combination of the three analyses using the amplitude method: variation of the oscillation amplitude A as a function of Δm_s. The *dashed line* corresponds to $A + 1.645\sigma_A$ with statistical uncertainties only, while the *dotted line* includes the contribution from systematics.

limit at 50% exclusion probability would correspond to $\Delta m_s > 5.3\,\text{ps}^{-1}$. The interval

$$8.2 < \Delta m_s < 9.4\,\text{ps}^{-1} \tag{24}$$

is also excluded at 95% C.L., where the exclusion probability varies between 25% and 19%. Applying procedure (b) defined in Section 5, the limit at 6.5 ps^{-1} goes down to 6.2 ps^{-1} and the region [8.2–9.4] ps^{-1} is no longer excluded.

References

[1] R. Aleksan, A. Le Yaouanc, L. Oliver, O. Pène and J.C. Raynal, Phys. Lett. B 316 (1993) 567.

[2] ALEPH Coll., D. Decamp et al., Phys. Lett. B 284 (1992) 177;
DELPHI Coll., P. Abreu et al., Phys. Lett. B 332 (1994) 488;
L3 Coll., M. Acciarri et al., Phys. Lett. B 335 (1994) 542;
OPAL Coll., R. Akers et al., Z. Phys. C 60 (1993) 199.

[3] ARGUS Coll., H. Albrecht et al., Phys. Lett. B 324 (1994) 249;
CLEO Coll., J. Bartelt et al., Phys. Rev. D50 (1994) 43.

[4] ALEPH Coll., D. Buskulic et al., Phys. Lett. B 313 (1993) 498;
ALEPH Coll., D. Buskulic et al., Phys. Lett. B 322 (1994) 441;
ALEPH Coll., D. Buskulic et al., Phys. Lett. B 356 (1995) 409;
ALEPH Coll., D. Buskulic et al., Phys. Lett. B 377 (1996) 205;
ALEPH Coll., D. Buskulic et al., Z. Phys. C 75 (1997) 397;
DELPHI Coll., P. Abreu et al., Phys. Lett B 338 (1994) 409;
DELPHI Coll., P. Abreu et al., Z. Phys. C 72 (1996) 17;
L3 Collab., M. Acciarri et al., Phys. Lett. B 383 (1996) 487;
OPAL Coll., R. Akers et al., Phys. Lett. B 327 (1994) 411;
OPAL Coll., R. Akers et al., Phys. Lett. B 336 (1994) 585;
OPAL Coll., R. Akers et al., Z. Phys. C 66 (1995) 555;
OPAL Coll., G. Alexander et al., Z. Phys. C 72 (1996) 377;
OPAL Coll., K. Ackerstaff et al., A Study of B Meson Oscillations Using Hadronic Z0 Decays Containing Leptons, CERN-PPE/97-036;
OPAL Coll., K. Ackerstaff et al., An Updated Study of B Meson Oscillations using Dilepton Events, CERN-PPE/97-064.

[5] DELPHI Coll., P. Abreu at al., Measurement of $B_d^0 \bar{B}_d^0$ oscillations, CERN-PPE 97-051.

[6] DELPHI Coll., P. Abreu et al., Nucl. Instr. and Meth. A 378 (1996) 57.

[7] N. Bingefors et al., Nucl. Instr. and Meth. A 328 (1993) 447;
V. Chabaud et al., Nucl. Instr. and Meth. A 368 (1996) 314.

[8] E.G. Anassontzis et al., Nucl. Instr. and Meth. A 323 (1992) 351.

[9] T. Sjöstrand, Comp. Phys. Comm. 82 (1994) 74.

[10] DELPHI Coll., P. Abreu et al., Z. Phys. C 73 (1996) 11.

[11] N. Isgur, D. Scora, B. Grinstein and M. Wise, Phys. Rev. D39 (1989) 799.

[12] H.G. Moser and A. Roussarie, Nucl. Instr. and Meth. A 384 (1997) 491.

[13] The LEP B Oscillation Working Group: LEP Combined Results on B^0 Oscillations: Update for the Summer 1997 Conferences, LEPBOSC NOTE 97/2,
ALEPH 97-083 PHYSIC 97-073, CDF Internal Note 4297,
DELPHI 97-135 PHYS 722, L3 Internal Note 2161,
OPAL Technical Note TN 502, SLD Physics Note 62.

[14] Particle Data Group, R.M. Barnett et al., Phys. Rev. D54 (1996) 1.

[15] DELPHI Coll., P. Abreu et al., Z. Phys. C 71 (1996) 11.

[16] G.V. Borisov and C. Mariotti, Nucl. Instr. and Meth. A 372 (1996) 181.

[17] The LEP Collaborations ALEPH, DELPHI, L3 and OPAL, the LEP Electroweak Working Group, and the SLD Heavy Flavour Group, A Combination of Preliminary Electroweak Measurements and Constraints on the Standard Model, prepared from contributions to the 28th International Conference on High Energy Physics, Warsaw, July 1996, CERN-PPE/96-183, December 6, 1996.